

Investigation of Developing Embryonic Morphology Using Optical Coherence Tomography

Stephen A. Boppart,^{*,†} Mark E. Brezinski,[‡] Brett E. Bouma,[†]
Guillermo J. Tearney,[†] and James G. Fujimoto^{†,1}

^{*}Harvard–MIT Division of Health Sciences and Technology and [†]Department of Electrical Engineering and Computer Science, Research Laboratory of Electronics, Massachusetts Institute of Technology, Cambridge, Massachusetts 02139; and [‡]Cardiac Unit, Massachusetts General Hospital, Harvard Medical School, Boston, Massachusetts 02114

Improved imaging of morphological changes has the potential of offering new insight into the complex process of embryonic development. Optical coherence tomography (OCT) is a new imaging technique for performing *in vivo* cross-sectional imaging of architectural morphology by measuring backscattered infrared light. This study investigates the application of OCT for imaging developing structure in *Rana pipiens*, *Xenopus laevis*, and *Brachydanio rerio*. Images are compared to conventional histological baselines. Cross-sectional imaging can be performed and structural morphology identified at greater imaging depths than possible with confocal and light microscopy. Repeated OCT imaging may be performed *in vivo* in order to track structural changes throughout development. © 1996 Academic Press, Inc.

INTRODUCTION

Imaging embryonic morphology that results from cellular differentiation is important for the understanding of genetic expression, regulation, and control. Several well-recognized imaging technologies are currently used to provide structural information about microscopic specimens. These include magnetic resonance imaging, computed-tomography, ultrasound, and confocal microscopy (CM).² High-resolution magnetic resonance imaging has been used to produce *in vivo* cross-sectional images of early *Xenopus laevis* development with resolutions of 12 μm (Jacobs and Fraser, 1994). Because the static and gradient magnetic fields required to obtain these resolutions are orders of magnitude greater than those found in most clinical systems, this modality represents a costly and technically challenging option that requires considerable skill from its operator in order to achieve high-resolution images. High-resolution computed-tomographic imaging of fixed insect specimens revealed internal microstructure with 8- to 12- μm resolution, yet required an elaborate microfocusing instrument and complex

image reconstruction algorithms (Morton *et al.*, 1990). Ultrasound backscatter microscopy utilizing high-frequencies (40–100 MHz) is capable of 50- μm resolutions to depths of 4–5 mm and has been applied to the analysis of early embryonic development in the mouse (Turnbull *et al.*, 1995). To effectively image with ultrasound, probes require contact with the tissue.

The invention of the confocal microscope (Minsky, 1988) and laser scanning confocal microscopy has produced a revolution of understanding of biological systems and their development largely due to the ability to selectively visualize biological specimens, cells, and subcellular constituents (White *et al.*, 1987). Transverse resolutions of 0.5 μm are typical with optical section thicknesses on the order of 1 μm (Webb *et al.*, 1990). Although CM is superb for optically sectioning a specimen, imaging depths are still limited to less than 1 mm in nontransparent tissue (Jester *et al.*, 1991). Recent advances in CM have successfully shown that *in vivo* confocal imaging is possible. Examples include the imaging of calcium dynamics in sea urchin eggs (Stricker *et al.*, 1992) as well as *Xenopus* oocytes (Girard and Clapham, 1993) during fertilization. Obtaining *in vivo* images is difficult, however, due to the toxicity of the products that are released when the fluorophores are excited by the incident laser radiation, the image acquisition time, and the maintenance of submicrometer specimen position. These limitations prevent biologists from imaging structure at later de-

¹ To whom correspondence should be addressed. Fax: (617) 253-9611. E-mail: jgfuj@mit.edu.

² Abbreviations used: OCT, optical coherence tomography; CM, confocal microscopy.

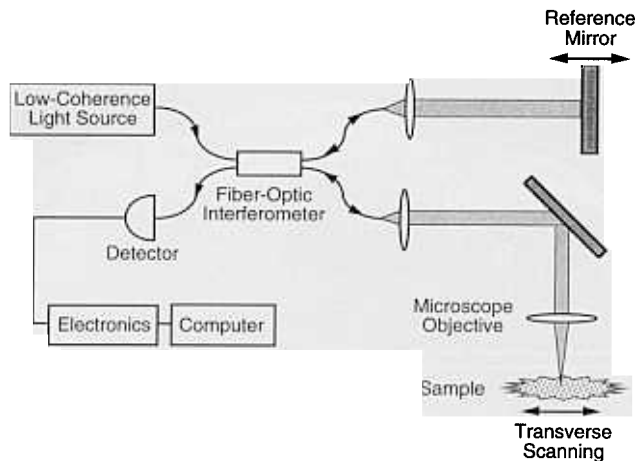


FIG. 1. Schematic diagram of the optical coherence tomography (OCT) imaging system. The compact OCT system uses a diode light source that is coupled into a fiber-optic beam splitter. Optical backscatter can be measured within the specimen with 10- to 15- μm resolution. Cross-sectional images are produced by scanning the specimen through the light beam while acquiring longitudinal (axial) reflectance profiles at each transverse position.

velopmental stages or in highly scattering, optically opaque specimens. Currently, internal morphological changes occurring in later stages can only be studied with histological preparations at discrete time points.

An *in vivo* means of imaging morphology is frequently needed to help identify the expression of genes. Furthermore, observing and tracking morphologic changes throughout development is useful for characterizing all aspects of genetic expression which take place. Optical coherence tomography (OCT) can perform high-resolution, noncontact, cross-sectional tomographic imaging *in vivo* with the potential to analyze the morphological changes in both semi-transparent and highly scattering specimens during normal and abnormal development. This paper investigates and demonstrates the potential of OCT for tomographic imaging in developmental biology. OCT tomographic imaging and histological correlations are performed on several of the commonly used animal models in order to establish baselines and demonstrate domains of application for this technology.

MATERIALS AND METHODS

Optical Coherence Tomography

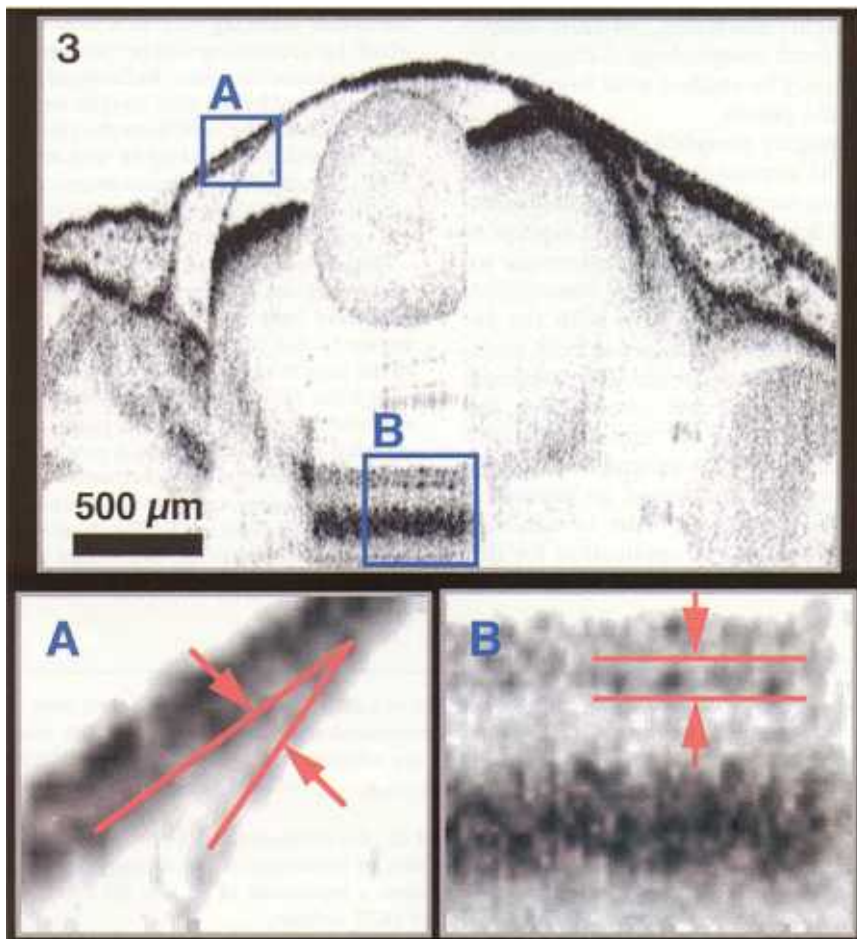
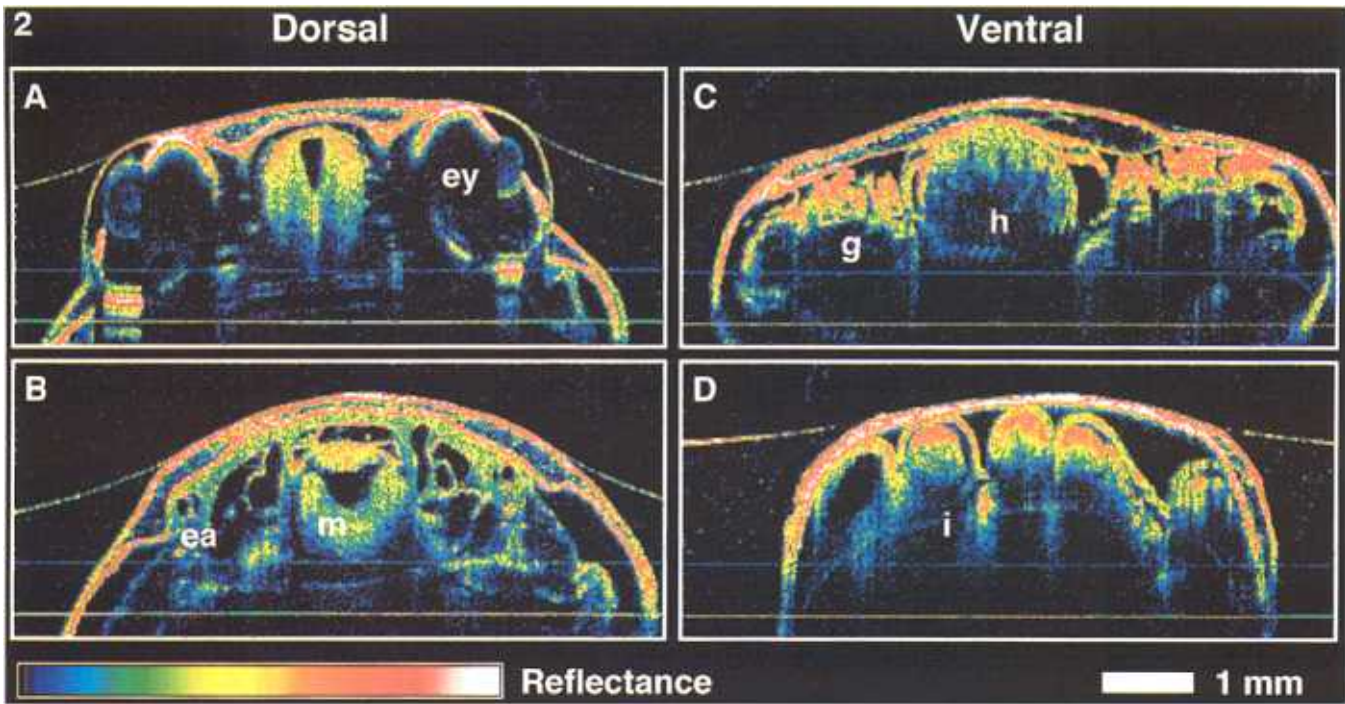
Optical coherence tomography is a new imaging modality that permits high-resolution, cross-sectional, tomographic imaging of architectural morphology of biological specimens *in vivo* (Huang *et al.*, 1991). The imaging technique is somewhat analogous to ultrasound-B mode imaging or radar except backscattering or reflections of light from biological structure are detected rather than acoustic reflections. Imaging is performed by directing a focused beam of light into the biological tissue and measuring the delay time (echo delay) for the backscattered light to return to the instrument. Light which is backscattered or reflected from structural features at varying depths within the specimen is measured to yield longitudinal (depth) information on tissue structures. A cross-sectional image of the specimen is constructed in a manner similar to radar imaging, by laterally scanning the light beam through the specimen and displaying longitudinal (depth) information from different adjacent transverse positions.

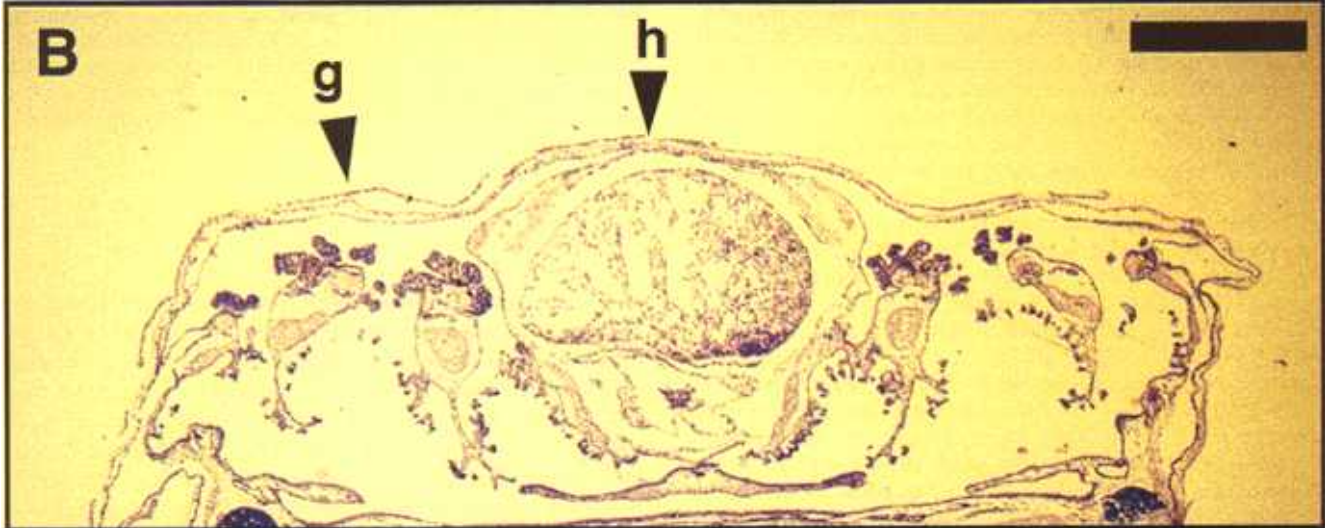
Because the velocity of light is extremely high, the echo delay time cannot be measured directly by electronics and an optical technique known as low-coherence interferometry is used. The measurement system consists of a low-coherent superluminescent diode light source in conjunction with a fiber optic Michelson-type interferometer. The low-coherence light is split equally by a fiber coupler with half sent to the reference arm and half sent to the sample arm of the interferometer as shown in Fig. 1. A computer-controlled scanning reference arm mirror sets the depths from which backscattering will be measured. Light from the sample arm is focused into the tissue. Reflections or backscatter from both arms is recombined by the fiber coupler and detected with a photodiode. Interference of the light from the two arms only occurs when their path lengths are matched to within the coherence length of the source. Thus, the coherence length of the source determines the longitudinal resolution. The transverse resolution is determined by the spot size of the incident beam within the tissue.

Optical coherence tomography has the ability to image specimens that are opaque to visible light because it utilizes wavelengths of light in the near-infrared region. Although most tissues appear opaque under visible light, they are relatively nonabsorbing in the near infrared. Imaging depth is therefore limited by attenuation from optical scattering rather than absorption. A 1300-nm superluminescent diode light source in the interferometer enables imaging to depths of up to 3 mm with an optical power of only 160 μW incident on the specimen. This imaging depth is sufficient for imaging many anatomical features of interest in most embryos and developing specimens. For these studies, the free-space longitudinal spatial resolution was 16 μm (as determined by the 50-nm optical bandwidth of the low-coherence light source) and the trans-

FIG. 2. Representative false-color cross-sectional OCT *in vitro* images of a *Rana pipiens* tadpole. Scans were taken from the (A, B) dorsal and (C, D) ventral sides of the specimen to emphasize particular anatomical structures. The specimen was partially submerged as is evident by the reflection at the air-liquid interface. Horizontal lines are artifacts from secondary backreflections from the imaging lens and have subsequently been eliminated. Abbreviations: ea, ear vesicle; ey, eye; g, internal gills; h, ventricle of heart; i, intestinal tract; m, medulla.

FIG. 3. Magnification of *Rana pipiens* eye globe to confirm predicted *in vivo* resolution of the OCT instrument. The *in vivo* resolution was predicted by dividing the free-space resolution by the average index of refraction of the specimen ($16 \mu\text{m}/1.35 = 12 \mu\text{m}$). (A) The cornea and lid could no longer be resolved as two structural layers below a separation of 15 μm . (B) The thickness of the ganglion cell layer is measured to be 14 μm , near the resolution limit of the current OCT system.





verse resolution was set to be 30 μm (as determined by the spot size of the light beam). Within the specimen, a longitudinal resolution of $\sim 12 \mu\text{m}$ is determined by dividing the free-space resolution by the measured average index of refraction of the specimen, $n = 1.35$ (Tearney et al., 1995).

The transverse resolution in OCT imaging is determined by the focusing parameters of the light beam in a manner similar to standard optical microscopy. In general, a tradeoff exists between magnification and depth of field. For a 30- μm transverse resolution, the resulting confocal parameter (depth of field) of the optical beam is 1.1 mm. If extremely high transverse resolutions are desired, then the resulting depth of field will be much shallower and it is necessary to scan the distance between the specimen and the lens during the imaging process. Thus, since our objective was to image architectural morphology, the focal spot size was set to be intermediate in order to obtain a large confocal parameter (depth of field).

The optical detection method used in OCT yields very high sensitivity. The system achieves a signal-to-noise ratio of 109 dB, defined by measuring the maximum signal when the optical beam is reflected from a high-reflecting mirror divided by the instrument noise level. This signal-to-noise ratio also determines the dynamic range which can be imaged. The fact that OCT uses low coherence light and detects light at selected echo time delays greatly discriminates against the detection of light which is multiply scattered. While confocal microscopy discriminates against unwanted light using spatial coherence, the technique is still sensitive to multiply scattered photons which degrade image quality (Izatt et al., 1994). In contrast to the on axis, en face, view that light microscopy provides, OCT permits the imaging of biological structure from the transverse, cross-sectional, perspective. Finally, OCT technology is based on fiber optics technology which is used in optical communication. Hence, the system is robust, compact, low cost, and can be readily integrated with current clinical and laboratory optical instruments including ophthalmic instrumentation (Hee et al., 1995), catheters, endoscopes, and modified light microscopes.

The clinical diagnostic potential of OCT has been demonstrated in the transparent tissue of the eye (Hee et al., 1995; Puliafito et al., 1995; Drexler et al., 1995) and for imaging pathology in highly scattering tissue due to its ability to reject multiply scattered photons (Schmitt et al., 1994; Fujimoto et al., 1995; Pan et al., 1995). OCT can image architectural morphology in tissue or specimens *in situ* without the need for excisional biopsy or to sacrifice. Studies *in vitro* (Brezinski et al., 1996) show considerable promise for the application of OCT to image coronary artery pathology. Thus, OCT can function as a type of "optical biopsy" or "optical histology."

Specimen Preparation

Imaging studies were performed on several standard biological animal models commonly employed in developmental biology investigations. OCT imaging was performed in *Rana pipiens* tadpoles (*in vitro*), *Brachydanio rerio* embryos and eggs (*in vivo*), and *X. laevis* tadpoles (*in vivo*).

A *R. pipiens* tadpole (stage 51) was euthanized by immersion in 0.05% benzocaine (Sigma Chemical Co.) for 30 min. The specimen

was then oriented for imaging by OCT (*in vitro*) with the optical beam incident from either the dorsal or ventral sides. After imaging, the specimen was fixed in 10% buffered formalin for 24 hr, embedded in paraffin, sectioned, and stained with hematoxylin and eosin.

A *B. rerio* embryo and egg at the 4-cell stage was partially submerged in low-temperature gelling agar and OCT imaged *in vivo* over a period of 24 hr. After imaging, the egg was released from the agar mounting and returned to the embryo medium.

X. laevis tadpoles (stage 47) were anesthetized by immersion in 0.05% tricaine (Sigma Chemical Co.) until they no longer responded to touch. *In vivo* OCT imaging was performed with the specimen immersed in water. Immediately following scanning, specimens were returned to their holding tank and allowed to recover. Specimens were sacrificed and processed for histology 2 hr following the image acquisition.

In order to facilitate the registration between OCT images and corresponding histology, numerous OCT images were first acquired at desired anatomical locations in 25- to 50- μm intervals. The position of the OCT measurement is known precisely because the specimen is on a micrometer precision stepping motor stage and the optical beam position is controlled by feedback-controlled precision galvanometers. In addition, serial sectioning at 20- μm intervals was performed during histological processing. Following light microscopic observations of the histology, OCT images from the same transverse plane in the specimen were selected based on correspondence to the histological sections. The animals used in this study were cared for and maintained under the established protocols.

RESULTS

To illustrate the ability of OCT to image developing internal morphology in optically opaque specimens, a series of cross-sectional images was acquired *in vitro* from the dorsal and ventral sides of a *R. pipiens* tadpole. The plane of the OCT image was perpendicular to the anteroposterior axis. Figure 2 shows representative OCT images displayed in false color. The color scale indicates the logarithm of the intensity of optical backscattering and spans a range of approximately -60 to -110 dB of the incident optical intensity. These high-resolution images ($7 \times 3 \text{ mm}$, 500×250 pixels, 12-bit) were acquired in 40 sec.

Features of internal architectural morphology are clearly visible in the images. Identifiable structures in Fig. 2B include the midbrain, fourth ventricle of the brain, and medulla as well as the ear vesicle. The horizontal semicircular canal and developing labyrinths are observed. Internal morphology not accessible in one orientation due to the specimen size or shadowing effects can be imaged by reorienting the specimen and scanning in the same cross-sectional image plane. The images in Figs. 2C and 2D were acquired with the OCT beam incident from the ventral side to image

FIG. 4. Corresponding histology of tadpole in Fig. 2. Histology, stained with hematoxylin and eosin (H&E), has strong correlation. Discrepancies are due to slight angular deviations of cross-sectional planes between histological preparation and OCT imaging. Note the histological preparation artifacts which can be identified after comparison with the OCT image. Bar, 1 mm.

the ventricle of the heart, internal gills, and gastrointestinal tract. The image of the eye (Fig. 2A) differentiates structures corresponding to the cornea, lens, and iris. The corneal thickness is on the order of 10 μm and can be resolved due to the differences in index of refraction between the water and the cornea. By imaging through the transparent lens, the incident OCT beam images several of the posterior ocular layers, including the ganglion cell layer, retinal neuroblasts, and choroid. The thicknesses of these layers were measured from the corresponding histology using a microscope with a calibrated reticule. The thicknesses of the ganglion cell layer, retinal neuroblasts, and choroid were 10, 80, and 26 μm , respectively, and demonstrate the high imaging resolution of the OCT system.

To confirm the *in vivo* resolution of this technique, the anterior chamber and the retinal layers of the eye globe were magnified and measured from the OCT image. Figure 3A illustrates that as the cornea and lid structures converge, two distinct layers could no longer be resolved when they were separated by less than 15 μm . The thickness of the retinal ganglion cell layer approaches the resolution limit of OCT and is measured in Fig. 3B to be 14 μm . These measurements confirm the *in vivo* resolution predicted by dividing the free-space resolution of the OCT instrument by the measured index of refraction of the specimen.

Retinal layers are not imaged throughout the entire globe because of shadowing effects from the highly backscattering iris and sclera which attenuate the transmission of light to deeper structures directly below. A sharp vertical boundary demarcates the regions where light is transmitted through the lens and where light is shadowed. Variation of the specimen orientation will vary the shadow orientation and permit the imaging of different internal structures.

OCT image contrast results from the different optical backscattering properties between different structures. Tissue structures are differentiated according to their varying degrees of optical backscattering (ranging from green, yellow, red, to white) while the fluid-filled cavities within the specimen have low backscattering (black to blue). The cartilaginous skeletal system of the tadpole appears highly scattering and is clearly identified in Fig. 2A. As light propagates deeper through the specimen, a larger percentage of the incident beam is either scattered or absorbed. Hence, less signal is available from deeper structures and the color of the structures appears shifted from red to green as the signal-to-noise ratio is reduced. Morphology located directly below a highly backscattering structure can be shadowed from the structure above. These effects are analogous to attenuation and shadowing observed in ultrasound. If the biological specimen is relatively homogeneous, the signal attenuation with depth can be compensated for by simple image processing techniques. However, because the morphology of the specimens used in this study are highly complex, the application of these techniques is problematic.

Figure 4 shows corresponding *R. pipiens* histology taken from the same axial plane as the OCT images. The neural retina, choroid, and sclera along with the anterior ocular structures in Fig. 4A confirm the morphology observed in Fig. 2A. The muscular ventricle of the heart in Fig. 4B is well correlated with the corresponding OCT image in Fig. 2C. Finally, in Fig. 4C, the multiple coils of the gastrointestinal tract confirm observations made from the OCT image in Fig. 2D.

There is a strong correlation of the tissue architectural morphology between OCT images and the histology. However, it is important to note that OCT images tissue properties in a completely different manner than histology. Histology relies on the differences in the transmission of light through stained tissue while OCT relies on differentials in optical backscattering. The resolution of OCT at present does not permit the imaging of subcellular features.

Figure 5 demonstrates the application of OCT for sequential imaging of development *in vivo*. Repeated images (3×3 mm, 300×300 pixels) were made of a developing zebrafish embryo within its egg beginning at 1 hr postfertilization, every 15 min, for 24 hr at the same cross-sectional plane within the specimen. Developmental changes illustrate early cleavage beginning at the 4-cell stage, 1 hr postfertilization. Because of the high mitotic rate of the embryo, results of cellular division and migration are observed as well as the establishment of the anterioposterior axis. In this example, the zebrafish egg and embryo were semitransparent and the use of OCT significantly complemented observations made using light microscopy. By imaging subtle differences in backscattering intensity, interfacial structural layers millimeters deep within specimens can be clearly delineated.

The advantages of OCT for developmental biology applications include the capability of distinguishing internal structural abnormalities from normal morphology. To demonstrate this point, Figs. 6A–6F compare and contrast *in vivo* morphology between both normal and abnormal *Xenopus* using OCT images (3×3 mm, 300×300 pixels) and corresponding histology. These developmental abnormalities are believed to be spontaneous and not the result of mutagenic agents. The normal *Xenopus* OCT image correlates well with histology. The neural tube shows normal formation as well as symmetrically placed and correctly oriented eyes. Internal gills are observed in both OCT and histology. Shadowing of the clay-lined dish is evident below the highly scattering ocular structure. In striking contrast, the abnormal specimen, at the same stage, has an irregularly shaped neural tube and abnormally large orbits which contain small, poorly formed optic cups. The optic cups are oriented asymmetrically. In this image plane, a longitudinal section of the left optic nerve and ocular muscles are noted by the arrow in Fig. 6C. An OCT image acquired more posterior in the abnormal specimen reveals the continuation of the poorly formed neural tube with morphological variations occurring on the scale of 50 μm . These images

the ventricle of the heart, internal gills, and gastrointestinal tract. The image of the eye (Fig. 2A) differentiates structures corresponding to the cornea, lens, and iris. The corneal thickness is on the order of 10 μm and can be resolved due to the differences in index of refraction between the water and the cornea. By imaging through the transparent lens, the incident OCT beam images several of the posterior ocular layers, including the ganglion cell layer, retinal neuroblasts, and choroid. The thicknesses of these layers were measured from the corresponding histology using a microscope with a calibrated reticule. The thicknesses of the ganglion cell layer, retinal neuroblasts, and choroid were 10, 80, and 26 μm , respectively, and demonstrate the high imaging resolution of the OCT system.

To confirm the *in vivo* resolution of this technique, the anterior chamber and the retinal layers of the eye globe were magnified and measured from the OCT image. Figure 3A illustrates that as the cornea and lid structures converge, two distinct layers could no longer be resolved when they were separated by less than 15 μm . The thickness of the retinal ganglion cell layer approaches the resolution limit of OCT and is measured in Fig. 3B to be 14 μm . These measurements confirm the *in vivo* resolution predicted by dividing the free-space resolution of the OCT instrument by the measured index of refraction of the specimen.

Retinal layers are not imaged throughout the entire globe because of shadowing effects from the highly backscattering iris and sclera which attenuate the transmission of light to deeper structures directly below. A sharp vertical boundary demarcates the regions where light is transmitted through the lens and where light is shadowed. Variation of the specimen orientation will vary the shadow orientation and permit the imaging of different internal structures.

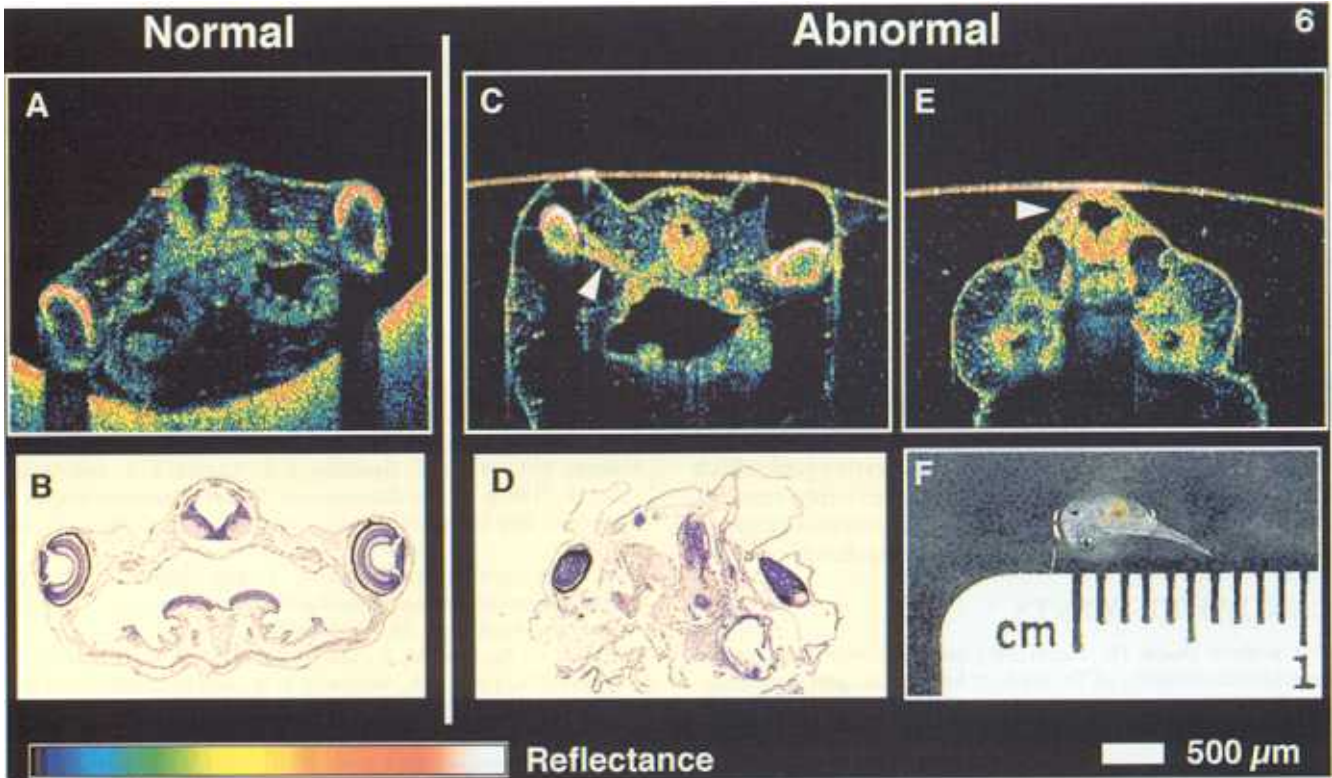
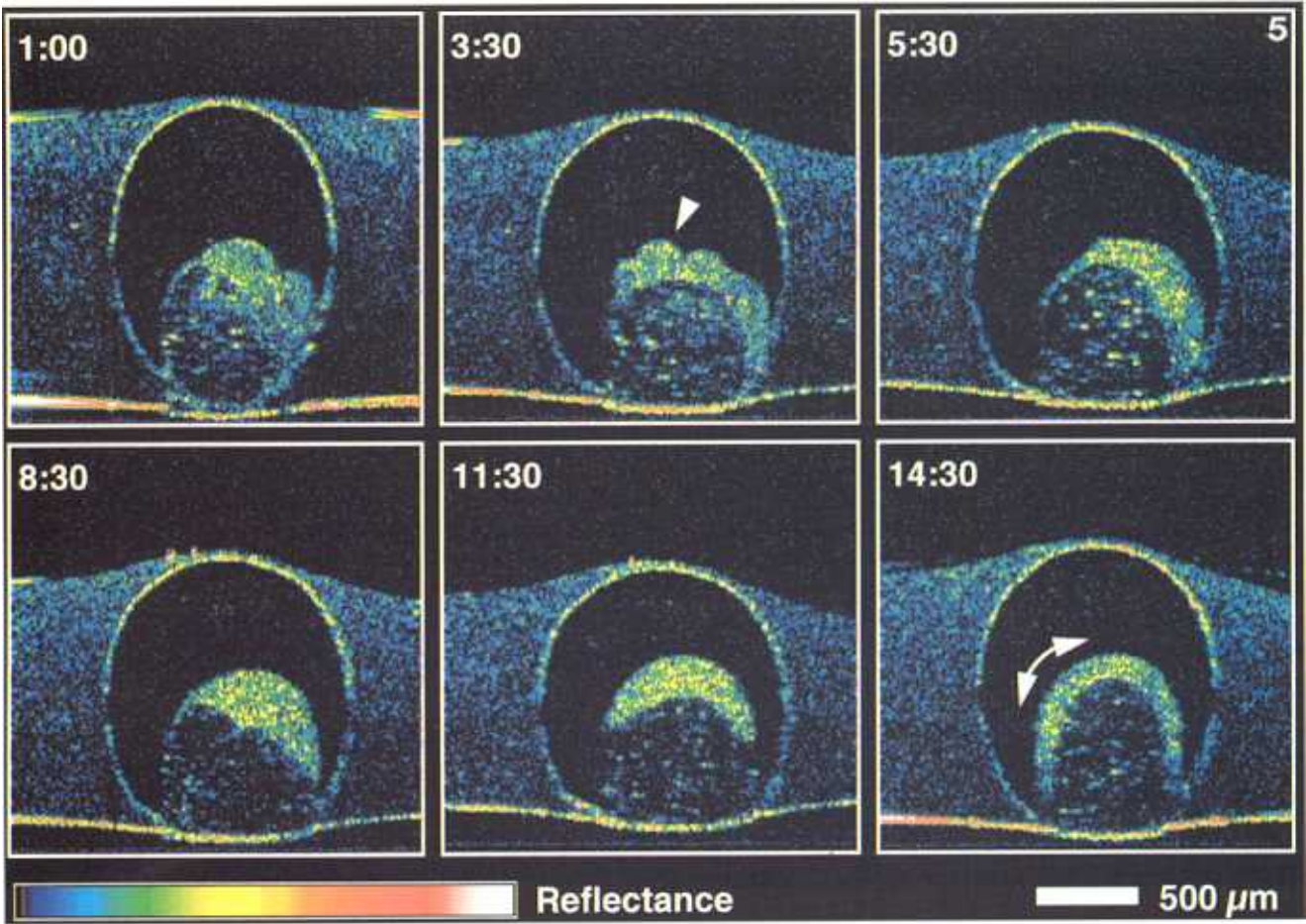
OCT image contrast results from the different optical backscattering properties between different structures. Tissue structures are differentiated according to their varying degrees of optical backscattering (ranging from green, yellow, red, to white) while the fluid-filled cavities within the specimen have low backscattering (black to blue). The cartilaginous skeletal system of the tadpole appears highly scattering and is clearly identified in Fig. 2A. As light propagates deeper through the specimen, a larger percentage of the incident beam is either scattered or absorbed. Hence, less signal is available from deeper structures and the color of the structures appears shifted from red to green as the signal-to-noise ratio is reduced. Morphology located directly below a highly backscattering structure can be shadowed from the structure above. These effects are analogous to attenuation and shadowing observed in ultrasound. If the biological specimen is relatively homogeneous, the signal attenuation with depth can be compensated for by simple image processing techniques. However, because the morphology of the specimens used in this study are highly complex, the application of these techniques is problematic.

Figure 4 shows corresponding *R. pipiens* histology taken from the same axial plane as the OCT images. The neural retina, choroid, and sclera along with the anterior ocular structures in Fig. 4A confirm the morphology observed in Fig. 2A. The muscular ventricle of the heart in Fig. 4B is well correlated with the corresponding OCT image in Fig. 2C. Finally, in Fig. 4C, the multiple coils of the gastrointestinal tract confirm observations made from the OCT image in Fig. 2D.

There is a strong correlation of the tissue architectural morphology between OCT images and the histology. However, it is important to note that OCT images tissue properties in a completely different manner than histology. Histology relies on the differences in the transmission of light through stained tissue while OCT relies on differentials in optical backscattering. The resolution of OCT at present does not permit the imaging of subcellular features.

Figure 5 demonstrates the application of OCT for sequential imaging of development *in vivo*. Repeated images (3×3 mm, 300×300 pixels) were made of a developing zebrafish embryo within its egg beginning at 1 hr postfertilization, every 15 min, for 24 hr at the same cross-sectional plane within the specimen. Developmental changes illustrate early cleavage beginning at the 4-cell stage, 1 hr postfertilization. Because of the high mitotic rate of the embryo, results of cellular division and migration are observed as well as the establishment of the anterioposterior axis. In this example, the zebrafish egg and embryo were semitransparent and the use of OCT significantly complemented observations made using light microscopy. By imaging subtle differences in backscattering intensity, interfacial structural layers millimeters deep within specimens can be clearly delineated.

The advantages of OCT for developmental biology applications include the capability of distinguishing internal structural abnormalities from normal morphology. To demonstrate this point, Figs. 6A–6F compare and contrast *in vivo* morphology between both normal and abnormal *Xenopus* using OCT images (3×3 mm, 300×300 pixels) and corresponding histology. These developmental abnormalities are believed to be spontaneous and not the result of mutagenic agents. The normal *Xenopus* OCT image correlates well with histology. The neural tube shows normal formation as well as symmetrically placed and correctly oriented eyes. Internal gills are observed in both OCT and histology. Shadowing of the clay-lined dish is evident below the highly scattering ocular structure. In striking contrast, the abnormal specimen, at the same stage, has an irregularly shaped neural tube and abnormally large orbits which contain small, poorly formed optic cups. The optic cups are oriented asymmetrically. In this image plane, a longitudinal section of the left optic nerve and ocular muscles are noted by the arrow in Fig. 6C. An OCT image acquired more posterior in the abnormal specimen reveals the continuation of the poorly formed neural tube with morphological variations occurring on the scale of 50 μm . These images



is not compromised because it relies on detecting deviations from the baseline.

The image scale and distortion effects are actually present in both ultrasound and MRI images although they arise from slightly different physics principles. Histology, to some extent, suffers from similar problems in obtaining measurements from preparations due to tissue preservation, dehydration, and sectioning. Tissue configuration following preparation may not always reflect the *in vivo* orientation, making quantification difficult. Despite the artifacts in both techniques, these artifacts are reproducible and can be perceived as the baseline. The differences in calibrating histopathology against real tissue dimensions usually does not compromise its diagnostic utility.

With further advances in OCT technology, improved discrimination and imaging of more detailed morphology should be possible. New laser sources at other wavelengths in the near infrared can enhance tissue contrast as well as potentially provide functional information since tissue scattering and absorbance properties in specimens are wavelength dependent. Shorter coherence length laser sources have been used to achieve higher longitudinal (axial) resolutions on the order of 2 to 4 μm (Clivaz et al., 1994; Bouma et al., 1995). OCT can be performed using a high numerical aperture lens to achieve high transverse resolutions, as in confocal microscopy, at the expense of reducing the depth of field (Izatt et al., 1994). With these higher resolutions, *in vivo* imaging of individual cells may be possible. Imaging time may be significantly reduced by increasing source power, scanning speed, and straightforward redesigning of electronics. Real-time acquisition of data will reduce the likelihood of specimen motion artifacts and may allow images to be obtained without the need for anesthesia. In combination with a specially designed endoscope, *in utero* imaging of embryonic and fetal development in live-bearing species may be possible.

Imaging developing embryonic morphology with OCT offers many new possibilities for studies in developmental biology as well as for microscopy in general. In this paper, we have shown that optical coherence tomography provides high-resolution morphological information on developing biology *in vivo* which can be correlated to known pathology based on histology. These results demonstrate the feasibility of gaining further insight into the morphological expression of the genetic program. High-resolution, *in vivo* optical histology using OCT permits the identification of morphological variations during embryogenesis. By tracking the results of cellular differentiation and rapidly identifying normal and abnormal organo- and morphogenesis in embryos, OCT represents a multifunctional investigative tool which will not only complement many of the existing imaging technologies available today, but also will potentially reveal previously unseen dynamic changes during development.

ACKNOWLEDGMENTS

The authors thank Dr. Hazel Sive and her co-workers at the Massachusetts Institute of Technology for providing us with *Xeno-*

pus laevis specimens and advice on the care and handling of embryos. The contributions of E. A. Swanson of MIT Lincoln Lab and J. F. Southern of Massachusetts General Hospital are also greatly appreciated. This work was supported by NIH Grant NIH-9-RO1-EY11289-10, the Office of Naval Research Medical Free Electron Laser Program Contract N00014-94-1-0717, the Air Force Office of Scientific Research Contract F49620-93-1-0301, and the Air Force Palace Knight Program.

REFERENCES

- Bouma, B. E., Tearney, G. J., Boppart, S. A., Hee, M. R., Brezinski, M. E., and Fujimoto, J. G. (1995). High resolution optical coherence tomographic imaging using a modelocked Ti:Al₂O₃ laser source. *Opt. Lett.* **20**, 1486–1488.
- Brezinski, M. E., Tearney, G. J., Bouma, B. E., Izatt, J. A., Hee, M. R., Swanson, E. A., Southern, J. F., and Fujimoto, J. G. (1996). Optical coherence tomography for optical biopsy: Properties and demonstration of vascular pathology. *Circulation* **93**, 1206–1213.
- Clivaz, X., Marquis-Weible, F., and Salathe, R-P. (1994). In European Biomedical Optics Conference, SPIE Proceedings, Vol. 2083, p. 19.
- Drexler, W., Hitzinger, C. K., Sattmann, H., and Fercher, A. F. (1995). Measurement of the thickness of fundus layers by partial coherence tomography. *Opt. Eng.* **34**, 701–710.
- Fujimoto, J. G., Brezinski, M. E., Tearney, G. J., Boppart, S. A., Bouma, B., Hee, M. R., Southern, J. F., and Swanson, E. A. (1995). Biomedical imaging and optical biopsy using optical coherence tomography. *Nature Med.* **1**, 970–972.
- Girard, S., and Clapham, D. (1993). Acceleration of intracellular calcium waves in *Xenopus* oocytes by calcium influx. *Science* **260**, 229–232.
- Hee, M. R., Izatt, J. A., Swanson, E. A., Huang, D., Schuman, J. S., Lin, C. P., Puliafito, C. A., and Fujimoto, J. G. (1995). Optical coherence tomography of the human retina. *Arch. Ophthalmol.* **113**, 326–332.
- Huang, D., Swanson, E. A., Lin, C. P., Schuman, J. S., Stinson, W. G., Chang, W., Hee, M. R., Flotte, T., Gregory, K., Puliafito, C. A., and Fujimoto, J. G. (1991). Optical coherence tomography. *Science* **254**, 1178–1181.
- Izatt, J. A., Hee, M. R., Owen, G. M., Swanson, E. A., and Fujimoto, J. G. (1994). Optical coherence microscopy in scattering media. *Opt. Lett.* **19**, 590–592.
- Jacobs, R. E., and Fraser, S. E. (1994). Magnetic resonance microscopy of embryonic cell lineages and movements. *Science* **263**, 681–684.
- Jester, J. V., Andrews, P. M., Petroll, W. M., Lemp, M. A., and Cavanagh, H. D. (1991). In vivo, real-time confocal imaging. *J. Electron Microsc. Technol.* **18**, 50–60.
- Minsky, M. (1988). Memoir on inventing the confocal scanning microscope. *Scanning* **10**, 128–138.
- Morton, E. J., Webb, S., Bateman, J. E., Clarke, L. J., and Shelton, C. G. (1990). Three-dimensional X-ray microtomography for medical and biological applications. *Phys. Med. Biol.* **35**, 805–820.
- Pan, Y., Birngruber, R., Rosperich, J., and Engelhardt, R. (1995). Low-coherence optical tomography in turbid tissue: Theoretical analysis. *Appl. Opt.* **34**, 6564–6574.
- Puliafito, C. A., Hee, M. R., Lin, C. P., Reichel, E., Schuman, J. S., Duker, J. S., Izatt, J. A., Swanson, E. A., and Fujimoto, J. G. (1995).

- Imaging of macular diseases with optical coherence tomography. *Ophthalmology* **120**, 217–229.
- Schmitt, J. M., Knuttel, A., Yadlowsky, M., and Eckhaus, M. A. (1994). Optical coherence tomography of a dense tissue: Statistics of attenuation and backscattering. *Phys. Med. Biol.* **39**, 1705–1720.
- Stricker, S. A., Centonze, V. E., Paddock, S. W., and Schatten, G. (1992). Confocal microscopy of fertilisation-induced calcium dynamics in sea urchin eggs. *Dev. Biol.* **149**, 370–380.
- Tearney, G. J., Brezinski, M. E., Southern, J. F., Bouma, B. E., Hee, M. R., and Fujimoto, J. G. (1995). Determination of the refractive index of highly scattering human tissue by optical coherence tomography. *Opt. Lett.* **20**, 2258–2260.
- Turnbull, D. H., Bloomfield, T. S., Baldwin, H. S., Foster, F. S., and Joyner, A. L. (1995). Ultrasound backscatter microscope analysis of early mouse embryonic brain development. *Proc. Natl. Acad. Sci. USA* **92**, 2239–2243.
- Webb, W. W., Wells, K. S., Sandison, D. R., and Strickler, J. (1990). Criteria for quantitative dynamical confocal fluorescence imaging. In "Optical Microscopy for Biology" (B. Herman and K. Jacobson, Eds.), pp. 73–108. Wiley-Liss, New York.
- White, J. G., Amos, W. B., and Fordham, M. (1987). An evaluation of confocal versus conventional imaging of biological structures by fluorescence light microscopy. *J. Cell Biol.* **105**, 41–48.

Received for publication November 15, 1995

Accepted March 21, 1996